COMMUNICATION

Relationship between penta-coordinated Al^{3+} site in the Al_2O_3 support and CH_4 combustion activity of Pd/Al_2O_3 catalyst

Received 00th January 20xx,
Accepted 00th January 20xx

DOI: 10.1039/x0xx00000x

Kazumasa Murata,[a] Takumi Shiotani,[a] Junya Ohyama,[bc] Ryutaro Wakabayashi,[d] Hirokazu Maruoka,[d] Tatsuo Kimura,[d] and Atsushi Satsuma*[ac]

Pd/Al_2O_3 catalysts were prepared using various Al_2O_3 supports with different structural features such as crystalline phase and crystallinity related to Al^{3+} coordination, revealing a significant insight on methane (CH_4) combustion activity of Pd nanoparticles with the fraction of penta-coordinated Al^{3+} sites in the Al_2O_3 supports.

CH_4 combustion is an important catalytic technology to remove CH_4 from exhaust gases, which can lead to serious greenhouse effects.[1] Supported Pd catalysts is known to be the most active for CH_4 combustion and have been extensively investigated.[2–10] However, in order to reduce Pd usage, the CH_4 combustion activity of supported Pd catalyst needs to be further improved.

Al_2O_3 is one of the most effective supports for Pd catalyst for CH_4 combustion.[11–13] A moderate charge transfer between Pd and Al_2O_3 tunes the redox properties of Pd particles.[11,14] Although Al_2O_3 has various crystalline phases, γ-Al_2O_3 has often been used as catalyst support because of its ability to highly disperse Pd species. The high dispersion is caused by not only the high specific surface area of γ-Al_2O_3, but also the immobilization of Pd species through the coordinately unsaturated penta-coordinated Al^{3+} (Al_{penta}) sites on γ-Al_2O_3(100).[15,16] On the other hand, the more thermally stable θ-Al_2O_3 and α-Al_2O_3 do not have Al_{penta} sites.[17] In other words, θ-Al_2O_3 and α-Al_2O_3 interact weakly with Pd species.

Recently, the tuning of the metal–support interaction (MSI) has received much attention in Pd/Al_2O_3 catalysts for CH_4 combustion.[14,18–22] The MSI varied with the Al_2O_3 crystalline phase causes structural changes in Pd particles prepared by the impregnation method.[18,19] Spherical or well-faceted Pd particles, which were highly active in methane combustion, were formed on θ-Al_2O_3 and α-Al_2O_3 with weak MSI. In contrast, due to the strong MSI, Pd particles on γ-Al_2O_3 form distorted shape having amorphous-like surface. Small Pd nanoparticles are also formed on three-dimensional structure of nanosheet-assembled Al_2O_3, where the Pd dispersion is maintained even at temperatures as high as 1000°C.[21] In addition, the surface modification by Al_2O_3 on supported Pd nanoparticles can enhance durability by inhibiting the thermal decomposition of PdO through the formation of Pd–O–Al bonds.[14,20] Therefore, the strength of the interaction between Pd and Al_2O_3 is expected to affect their redox properties of Pd/Al_2O_3 catalyst at lower temperatures. However, the effect of Al_2O_3 structure on the CH_4 combustion activity of Pd/Al_2O_3 at low temperatures is not well understood.

Herein, CH_4 combustion activity of colloidal Pd nanoparticles (NPs) were systematically investigated through deposition over crystalline Al_2O_3 supports (γ-Al_2O_3, θ-Al_2O_3, and α-Al_2O_3). To enhance the significance of its MSI behaviour, we further utilized mesoporous Al_2O_3 (m-Al_2O_3) prepared using amphiphilic organic molecules.[23] The alumina frameworks can be designed from amorphous to partially crystalline (γ-phase) by elevating calcination temperature.[24,25] Actually, the coordination structure of Al^{3+} sites was changed distinctly, which was confirmed by using ^{27}Al magic angle spinning (MAS) nuclear magnetic resonance (NMR) spectroscopy. Based on the relationship between CH_4 combustion activity of Pd/Al_2O_3 and structural parameter of the Al_2O_3 supports, we found that the coordination structure of Al^{3+} sites was quite important for understanding CH_4 combustion activity related to Pd redox property.

[a] Graduate School of Engineering, Nagoya University, Nagoya 464-8603, Japan. E-mail: satsuma@chembio.nagoya-u.ac.jp
[b] Faculty of Advanced Science and Technology, Kumamoto University, Kumamoto 860-8555, Japan.
[c] Elements Strategy Initiative for Catalysts and Batteries (ESICB), Kyoto University, Katsura, Kyoto 615-8520, Japan.
[d] National Institute of Advanced Industrial Science and Technology (AIST) Shimoshidami, Moriyama-ku, Nagoya 463-8560, Japan.
Electronic Supplementary Information (ESI) available: [details of any supplementary information available should be included here]. See DOI: 10.1039/x0xx00000x

Table 1 Structural parameters of Al_2O_3 supports.

sample	crystalline phase	S_{BET} ($m^2\ g^{-1}$)	Fraction of		
			Al_{octa} site	Al_{penta} site	Al_{tetra} site
γ-Al_2O_3	γ	140	0.628	0.041	0.331
θ-Al_2O_3	θ	73	0.609	0	0.391
α-Al_2O_3	α	10	1	0	0
m-Al_2O_3-1, calcined at 550 °C	amorphous	490	0.372	0.295	0.333
m-Al_2O_3-2, calcined at 700 °C	partially γ	340	0.619	0.126	0.255
m-Al_2O_3-3, calcined at 850 °C	partially γ	320	0.655	0.093	0.252

Structural features of Al_2O_3 supports used in this study are summarized in Table 1, which were analyzed through N_2 adsorption-desorption, X-ray diffraction (XRD) and ^{27}Al MAS NMR measurements. The experimental details were described in the supporting information. For example, the specific surface area of α-Al_2O_3 was the smallest (10 $m^2\ g^{-1}$) and that of m-Al_2O_3-1 was the largest (490 $m^2\ g^{-1}$) among them (Fig. S1). As shown in Fig. S2, the XRD patterns of γ-, θ-, and α-Al_2O_3 were identified typical γ, θ, and α phases, respectively. No specific XRD peaks were detected in the XRD pattern of m-Al_2O_3-1, indicating that m-Al_2O_3-1 is in an amorphous structure. The XRD patterns of m-Al_2O_3-2 and -3 showed very weak diffraction peaks derived by the formation of its γ-phase, indicating m-Al_2O_3-2 and 3 were nearly amorphous but contained crystallites of γ-Al_2O_3 in part.

Fig. 1 shows ^{27}Al MAS NMR spectra of the Al_2O_3 supports. The NMR peaks of γ-Al_2O_3 observed at 0, 35, and 70 ppm were derived from octahedral Al^{3+} (Al_{octa}), Al_{penta}, and tetrahedral Al^{3+} (Al_{tetra}) sites, respectively.[15,17,20–22,26] The fractions of Al^{3+} sites with different coordination structure can be quantitatively analyzed by Gaussian fitting (Fig. S3). The fraction of Al_{octa} and Al_{tetra} site in γ-Al_2O_3 were 0.628 and 0.332, respectively, being in agreement with the previous report.[27] This result indicates that the bulk structure of γ-Al_2O_3 is mainly a spinel structure with Al^{3+} vacancies in the octahedral positions. The presence of Al_{penta} sites has been reported to be existed on the (100) surface of γ-Al_2O_3.[15,17] The NMR spectrum of θ-Al_2O_3 exhibited the presence of Al_{octa} and Al_{tetra} sites, with the absence of Al_{penta} sites. The NMR spectrum of α-Al_2O_3 with the most stable corundum-type structure, represented the presence of Al_{octa} sites only.[28] In cases of m-Al_2O_3, compared to γ-Al_2O_3, the NMR peak intensity assigned to Al_{penta} sites was much increased than that observed for γ-Al_2O_3 (the fraction of Al_{penta}; 0.041). The fractions of the Al_{penta} sites in m-Al_2O_3-1, m-Al_2O_3-2, and m-Al_2O_3-3 were 0.295, 0.126, and 0.093, respectively, revealing that coordinatively unsaturated Al_{penta} sites were abundant in such Al_2O_3 supports with low crystallinity.

Pd NPs were synthesized by a modified colloidal method, originally reported by Cargnello et al.[29], in order to eliminate the size effect of Pd catalyst on in CH_4 combustion.[12,18] The detailed procedure is described in the supporting information. The Pd NPs were then deposited on the aforementioned Al_2O_3 supports where the amount of Pd loaded was 1 wt %. Fig. 2 shows TEM images of Pd/Al_2O_3 with size distributions of Pd NPs. All the size distributions of Pd NPs were narrow with average size of 3–4 nm. Comparison of the ^{27}Al MAS NMR spectra of m-Al_2O_3-3 with and without Pd NPs revealed a decrease in the

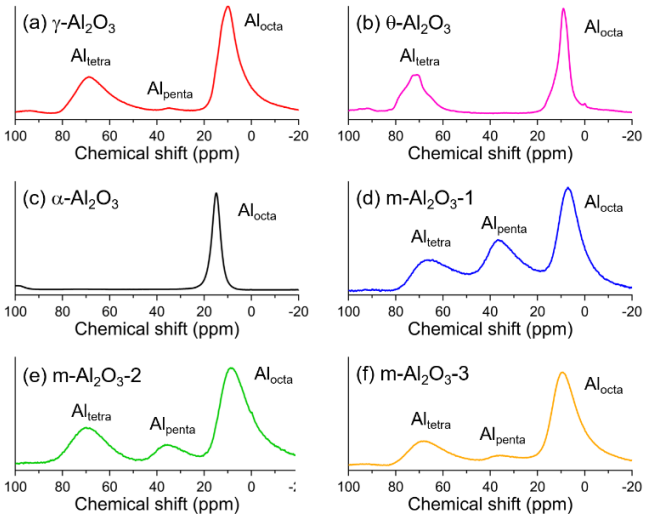

Fig. 1 ^{27}Al MAS NMR spectra of Al_2O_3 supports. (a) γ-Al_2O_3, (b) θ-Al_2O_3, (c) α-Al_2O_3, (d) m-Al_2O_3-1, (e) m-Al_2O_3-2, and (f) m-Al_2O_3-3. NMR peaks around 10, 35, and 70 ppm were assigned to Al_{octa}, Al_{penta}, and Al_{tetra} sites, respectively.

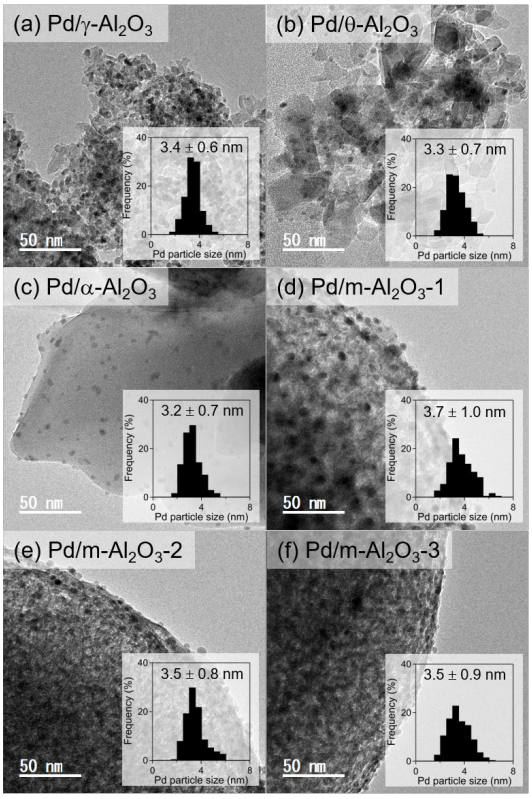

Fig. 2 TEM images of Pd/Al_2O_3 catalyst and their size distribution histograms. (a) Pd/γ-Al_2O_3, (b) Pd/θ-Al_2O_3, (c) Pd/α-Al_2O_3, (d) Pd/m-Al_2O_3-1, (e) Pd/m-Al_2O_3-2, and (f) Pd/m-Al_2O_3-3.

amount of Al_{penta} sites after the loading of Pd NPs, meaning that some Al_{penta} sites were utilized for interacting with Pd NPs (Fig. S4).[15]

Fig. 3a shows CH_4 combustion activity of Pd/α-Al_2O_3, Pd/θ-Al_2O_3 and Pd/γ-Al_2O_3 catalysts. It should be noted that the influence of surface Pd amount can be ignored in CH_4 conversion since the Pd dispersions (31.9–34.9%) estimated from the TEM were almost the same. Pd/α-Al_2O_3, Pd/θ-Al_2O_3 and Pd/γ-Al_2O_3 catalysts were highly active for CH_4 combustion comparable to previous reports.[2,4,6,18,20,21] Their light-off temperature was around 250 °C and CH_4 conversion was reached almost up to 100% at 400 °C. Fig. 3b also shows CH_4 combustion activities of three Pd/m-Al_2O_3 with that observed for Pd/γ-Al_2O_3. As the calcination temperature of m-Al_2O_3 decreased (in the order of m-Al_2O_3-3, m-Al_2O_3-2, and m-Al_2O_3-1), according to crystallinity (γ-phase) of the Al_2O_3 frameworks, the light-off temperature of CH_4 combustion was shifted from 440 °C (m-Al_2O_3-1) to 400 °C (m-Al_2O_3-2) and 300 °C (m-Al_2O_3-3). Considering the same size of the Pd particles, the difference in the light-off temperature suggested a change in the nature of the active Pd/PdO phase. It should be noted that CH_4 combustion activity of Al_2O_3 itself at 200–600 °C is negligible.[11]

The relationship between structure of Al_2O_3 supports and CH_4 combustion activity of Pd/Al_2O_3 was investigated. Despite the difference in crystalline phase between γ-Al_2O_3, θ-Al_2O_3, and α-Al_2O_3, there was little difference in CH_4 combustion activity of Pd/Al_2O_3. Fig. 4 is a summary of T_{50} of the Pd/Al_2O_3 catalysts as a function of the fraction of Al_{penta} site in the Al_2O_3 supports. T_{50} was the temperature when the CH_4 conversion reached 50% and was used as a measure of the CH_4 combustion activity of Pd/Al_2O_3. The T_{50} value was decreased monotonically with the fraction of the Al_{penta} site. In contrast, no clear relationship was obtained between the T_{50} value and the fraction of Al_{tetra} and Al_{octa} sites (Fig. S5). Therefore, the fraction of the Al_{penta} site in the Al_2O_3 supports was proposed as a controlling factor for CH_4 combustion over Pd/Al_2O_3 catalyst.

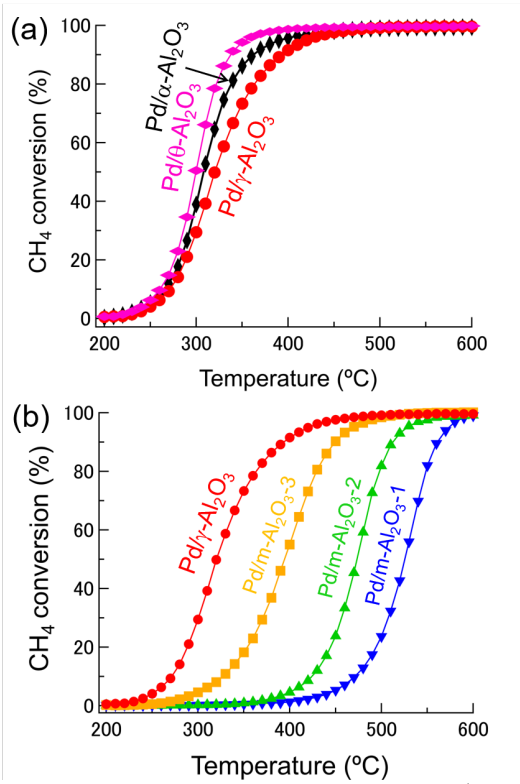

Fig. 3 CH_4 conversion as a function of temperature over various Pd/Al_2O_3 catalysts prepared by using (a) crystalline Al_2O_3 and (b) mesoporous Al_2O_3.

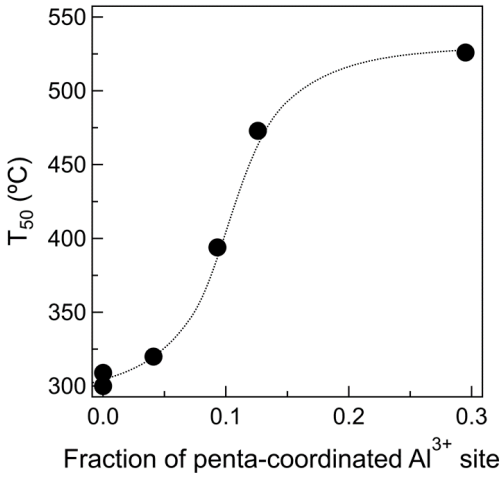

Fig. 4 Relationship between CH_4 combustion activity and fraction of penta-coordinated Al^{3+} site of Al_2O_3.

During CH_4 combustion, Pd particles were easily oxidized to form active PdO phase[10,30,31] and CH_4 was oxidized by the lattice oxygen of PdO via the Mars-van-Kreveren mechanism.[3,32] In fact, according to X-ray photoelectron spectroscopy (XPS), Pd particles on Al_2O_3 supports was almost completely oxidized to PdO during CH_4 combustion (Fig. S6). Therefore, the PdO particles anchoring on abundant Al_{penta} sites can be inactive for CH_4 combustion due to the suppression of Pd redox property. In order to investigate the ease of reduction of PdO phase in Pd/Al_2O_3, the temperature programmed reduction by CH_4 (CH_4-TPR) was performed (Fig. S7). The formation of CO_2 derived from the complete oxidation of CH_4 over PdO was observed at 240–350 °C.[11] The lower reduction temperature of PdO in Pd/Al_2O_3, the higher the CH_4 combustion activity. There was no difference in the ease of oxidation of Pd in Pd/Al_2O_3 (Fig. S8). For the Pd/Al_2O_3 catalysts, Pd particles form bonds with Al atoms and adjacent O atoms on the Al_2O_3 surface. According to previous reports, the metal species positively and negatively charge via the metal–Al and metal–O bonds, respectively.[33–35] Therefore, it is suggested that the reducibility of PdO particles was suppressed by the charge transfer from Pd to O atoms. Moreover, as the coordinatively unsaturated Al^{3+} sites and the adjacent O atoms function as stronger Lewis acid-base sites, m-Al_2O_3 supports with the high fraction of Al_{penta} sites are possible to strongly interact with Pd.[34,36] In the previous study,[20] the strong interaction between Al_{penta} sites and PdO phase inhibited the thermal decomposition of PdO at high temperatures (> 800 °C), resulting in high thermal durability. The results in this study conclude that the presence of abundant Al_{penta} sites reduce the reducibility of PdO phase by CH_4 at low temperatures (< 600 °C).

In summary, we investigated the effect of local structure of Al_2O_3 supports on CH_4 combustion activity arising from Pd NPs deposited over the Al_2O_3 supports. Among the structural parameters including crystalline phase and coordination structure of Al^{3+} site, the coordination structure, more specifically its Al_{penta} site is strongly correlated to the catalytic activity because the strong interaction of the Al_{penta} site with Pd NPs changes the reducibility of PdO. PdO species on Al_2O_3 with the low fraction of Al_{penta} sites were reduced at low temperature and thus highly active for CH_4 combustion. In this context, this study shows for the first time that the structure of Al_2O_3, in particular, the fraction of Al_{penta} site affects the redox property of Pd NPs as well as CH_4 combustion activity of Pd/Al_2O_3.

This work was partly supported by the JSPS KAKENHI Grant Number 18H01787 and 19J15440 from the Ministry of Education, Culture, Sports, Science and Technology (MEXT), Japan. The authors acknowledge the NU-AIST alliance project. A portion of this work was performed under management of the Elements Strategy Initiative for Catalysts & Batteries (ESICB), which is also supported by MEXT.

Conflicts of interest

There are no conflicts to declare.

References

1 R. J. Farrauto, *Science*, 2012, **337**, 659–660.
2 M. Cargnello, J. J. D. Jaen, J. C. H. Garrido, K. Bakhmutsky, T. Montini, J. J. C. Gamez, R. J. Gorte and P. Fornasiero, *Science*, 2012, **337**, 713–717.
3 Y.-H. C. Chin, C. Buda, M. Neurock and E. Iglesia, *J. Am. Chem. Soc.*, 2013, **135**, 15425–42.
4 M. Danielis, S. Colussi, C. deLeitenburg, L. Soler, J. Llorca and A. Trovarelli, *Angew. Chem. Int. Ed.*, 2018, 10212–10216.
5 H. Peng, C. Rao, N. Zhang, X. Wang, W. Liu, W. Mao, L. Han, P. Zhang and S. Dai, *Angew. Chem. Int. Ed.*, 2018, **57**, 8953–8957.
6 A. W. Petrov, D. Ferri, F. Krumeich, M. Nachtegaal, J. A. Van Bokhoven and O. Kröcher, *Nat. Commun.*, 2018, **9**, 2545.
7 E. D. Goodman, S. Dai, A.-C. Yang, C. J. Wrasman, A. Gallo, S. R. Bare, A. S. Hoffman, T. F. Jaramillo, G. W. Graham, X. Pan and M. Cargnello, *ACS Catal.*, 2017, 4372–4380.
8 J. J. Willis, E. D. Goodman, L. Wu, A. R. Riscoe, P. Martins, C. J. Tassone and M. Cargnello, *J. Am. Chem. Soc.*, 2017, **139**, 11989–11997.
9 Y. Mahara, J. Ohyama, T. Tojo, K. Murata, H. Ishikawa and A. Satsuma, *Catal. Sci. Technol.*, 2016, **6**, 1–10.
10 Y. Mahara, T. Tojo, K. Murata, J. Ohyama and A. Satsuma, *RSC Adv.*, 2017, **7**, 34530–34537.
11 K. Murata, D. Kosuge, J. Ohyama, Y. Mahara, Y. Yamamoto, S. Arai and A. Satsuma, *ACS Catal.*, 2020, **10**, 1381–1387.
12 J. J. Willis, A. Gallo, D. Sokaras, H. Aljama, S. H. Nowak, E. D. Goodman, L. Wu, C. J. Tassone, T. F. Jaramillo, F. Abild-pedersen and M. Cargnello, *ACS Catal.*, 2017, **7**, 7810–7821.
13 H. Yoshida, T. Nakajima, Y. Yazawa and T. Hattori, *Appl. Catal. B Environ.*, 2007, **71**, 70–79.
14 J. Yang, M. Peng, G. Ren, H. Qi, X. Zhou, J. Xu, F. Deng, Z. Chen, J. Zhang, K. Liu, X. Pan, W. Liu, Y. Su, W. Li, B. Qiao, D. Ma and T. Zhang, *Angew. Chem. Int. Ed.*, 2020, anie.202009050.
15 J. H. Kwak, J. Hu, D. Mei, C.-W. Yi, D. H. Kim, C. H. F. Peden, L. F. Allard and J. Szanyi, *Science*, 2009, **325**, 1670–1673.
16 D. Mei, J. H. Kwak, J. Hu, S. J. Cho, J. Szanyi, L. F. Allard and C. H. F. Peden, *J. Phys. Chem. Lett.*, 2010, **1**, 2688–2691.
17 R. Wischert, P. Florian, C. Copéret, D. Massiot and P. Sautet, *J. Phys. Chem. C*, 2014, **118**, 15292–15299.
18 K. Murata, Y. Mahara, J. Ohyama, Y. Yamamoto, S. Arai and A. Satsuma, *Angew. Chemie Int. Ed.*, 2017, **56**, 15993–15997.
19 K. Murata, J. Ohyama, Y. Yamamoto, S. Arai and A. Satsuma, *ACS Catal.*, 2020, **10**, 8149–8156.
20 H. Duan, R. You, S. Xu, Z. Li, K. Qian, T. Cao, W. Huang and X. Bao, *Angew. Chemie Int. Ed.*, 2019, **58**, 12043–12048.
21 X. Yang, Q. Li, E. Lu, Z. Wang, X. Gong, Z. Yu, Y. Guo, L. Wang, Y. Guo, W. Zhan, J. Zhang and S. Dai, *Nat. Commun.*, 2019, **10**, 1611.
22 J. Lin, X. Chen, Y. Zheng, F. Huang, Y. Xiao, Y. Zheng and L. Jiang, *Catal. Sci. Technol.*, 2020, **10**, 4612–4623.
23 H. Maruoka, A. Tomita, L. Zheng and T. Kimura, *Langmuir*, 2018, **34**, 13781–13787.
24 T. Kimura and H. Maruoka, *Chem. Commun.*, 2019, **55**, 10003–10006.
25 H. Maruoka and T. Kimura, *Bull. Chem. Soc. Jpn.*, 2019, **92**, 1859–1866.
26 J. Lee, H. Jeon, D. G. Oh, J. Szanyi and J. H. Kwak, *Appl. Catal. A Gen.*, 2015, **500**, 58–68.
27 R. Prins, *Angew. Chemie Int. Ed.*, 2019, **58**, 15548–15552.
28 G. Busca, *Catal. Today*, 2014, **226**, 2–13.
29 M. Cargnello, C. Chen, B. T. Diroll, V. V. T. Doan-Nguyen, R. J. Gorte and C. B. Murray, *J. Am. Chem. Soc.*, 2015, **137**, 6906–6911.
30 Y. H. C. Chin, M. García-Diéguez and E. Iglesia, *J. Phys. Chem. C*, 2016, **120**, 1446–1460.
31 S. K. Matam, M. H. Aguirre, A. Weidenkaff and D. Ferri, *J. Phys. Chem. C*, 2010, **114**, 9439–9443.
32 M. Van den Bossche and H. Grönbeck, *J. Am. Chem. Soc.*, 2015, **137**, 12035–12044.
33 C. Chizallet, P. Sautet and P. Raybaud, *ACS Catal.*, 2012, **2**, 1346−1357.
34 M. C. Valero, P. Raybaud and P. Sautet, *J. Phys. Chem. B*, 2006, **110**, 1759–1767.
35 V. R. Cooper, A. M. Kolpak, Y. Yourdshahyan and A. M. Rappe, *Phys. Rev. B - Condens. Matter Mater. Phys.*, 2005, **72**, 1–4.
36 R. Wischert, C. Copéret, F. Delbecq and P. Sautet, *Angew. Chem. Int. Ed.*, 2011, **50**, 3202–3205.

